Proceedings of the Thirty-sixth (2026) International Ocean and Polar Engineering Conference **www.isope.org**
Orlando, Florida, USA, May 31-June 5, 2026

ISBN 978-1-880653-72-2; ISSN 1098-6189

Flow Field Prediction Around the S826 Airfoil Based on Graph Neural Network

Yisheng Yao[1], Haiting Yu[2], Maokun Ye[1], Decheng Wan[1]*

[1] Computational Marine Hydrodynamics Lab (CMHL), School of Ocean and Civil Engineering,
Shanghai Jiao Tong University, Shanghai, China
[2] Wuhan Second Ship Design and Research Institute, Wuhan, China
*Corresponding author

ABSTRACT

The Actuator Line Method (ALM) has become one of the most popular numerical techniques for aerodynamic analysis and performance prediction of wind turbines. Nevertheless, the prediction accuracy of ALM is strongly affected by the quality of airfoil lift and drag databases, which are commonly obtained through costly and time-consuming wind tunnel tests or time-intensive 2D-CFD simulations. In addition, traditional databases only provide aerodynamic coefficients at discrete angles of attack, and interpolation has to be adopted in practical calculations, which inevitably introduces extra errors and reduces the reliability of ALM results. To solve these problems, this paper proposes a novel surrogate model combining a convolutional neural network with an attention mechanism (CNN-Attention). The model is trained using high-fidelity 2D-CFD flow field data under discrete angles of attack after proper preprocessing and normalization. It can quickly and accurately predict the flow field distribution around airfoils at any given angle of attack with much higher computational efficiency than conventional CFD methods. Based on the predicted flow fields, high-precision lift and drag coefficients can be directly calculated via integration, which effectively avoids the errors caused by discrete databases. The proposed model achieves an excellent balance between computational efficiency and accuracy, providing reliable aerodynamic data support for wind turbine wake simulation and performance optimization, and also presenting a new approach for the aerodynamic design of advanced blade airfoils.

KEY WORDS: Wind turbine; aerodynamic performance; CFD; CNN-Attention; surrogate model;

INTRODUCTION

Actuator Line Method (ALM) (Sørensen 2002) is mainly applied in wind power industry-related numerical simulation and computational research, especially in wind turbine wake flow simulation and wind farm power generation efficiency prediction. This advanced numerical method was proposed to address the critical issue that traditional computational fluid dynamics (CFD) (Ye 2023) methods consume enormous computational resources and require extremely long calculation cycles when fully modeling the complex geometric structure of wind turbine blades, including their surface details, twist angles, and chord length variations (Peters 2024). Thus, ALM introduces a virtual volume-distributed actuator line, usually arranged along the span wise direction of the wind turbine blade, to equivalently represent actual blades; this virtual line simulates the aerodynamic effect of blade rotation on the downstream wake flow field by applying concentrated aerodynamic forces, avoiding detailed blade surface mesh division and significantly reducing computational costs. Currently, as one of the most mature and widely adopted theories in commercial CFD software for wind turbine wake-related research (Giordani 2023), it is widely used in wind turbine design optimization, wind farm layout planning, and adjacent wind turbine wake interference research.

When using ALM for blade aerodynamic simulation, calling the lift and drag database of the blade's corresponding airfoil is crucial, as airfoil lift and drag characteristics are directly related to key factors such as airfoil geometric parameters (e.g., camber, thickness, and leading/trailing edge shape), Reynolds number (determined by incoming flow velocity and airfoil chord length), and angle of attack (the angle between incoming flow direction and airfoil chord line). In practical engineering, most airfoil aerodynamic data in commercial wind turbines and research projects are obtained from wind tunnel measurement experiments (Jonkman 2003), the most reliable data source in aerodynamic research. For example, airfoil aerodynamic data for some NREL series wind turbines, such as the NACA E387 airfoil and the S822 airfoil, are publicly available and widely used in academic and engineering practice due to high reliability (Selig 2001).

Though wind tunnel measurement data have high accuracy and authenticity, they have obvious limitations: new or modified airfoils require complex, costly experimental tests, consuming considerable human, material, and financial resources with a long cycle (usually several months to more than a year). Additionally, wind tunnel data are discrete, measuring lift and drag coefficients only at specific angles of attack and Reynolds numbers rather than continuous data over the full applicable range. Thus, ALM-based CFD calculations often require interpolation to obtain aerodynamic parameters at unmeasured conditions, which introduces additional errors; interpolated data accuracy decreases with larger intervals, affecting wake simulation accuracy.

To address these problems, an alternative is two-dimensional CFD calculations for specific angles of attack of the target airfoil (Ye 2023b); after obtaining detailed airfoil surrounding flow field distribution via 2D simulations, lift and drag coefficients are computed by integrating surface pressure and shear stress distributions. This method is convenient and flexible—no expensive equipment is needed, and aerodynamic results for arbitrary applicable angles of attack can be quickly obtained by adjusting simulation parameters. However, it requires numerous 2D CFD simulations before each wake calculation (to cover the full blade operation angle of attack range), resulting in high computational costs and failing to fundamentally solve low efficiency.

With the rapid development of artificial intelligence, surrogate models and data-driven methods have made significant progress in aerodynamic simulation (He 2022). For example, Wang researched wind turbine wake region reconstruction based on ANN, CNN and U-Net, splitting the wake into subdomains for separate training and integrating models to predict the wake field; this reduced wake velocity prediction error but not turbulence intensity error, and subdomain boundary processing's consistency with flow field physical characteristics remains debatable (Wang 2022). David proposed DeepWFLO, a deep convolutional hierarchical encoder-decoder neural network, as an image-to-image surrogate model for wind velocity field prediction in wind farm layout optimization (WFLO), using a dataset of wind turbine layouts, undisturbed flow fields, and wake-included velocity fields generated by analytical wake models and CFD simulations (David 2024).

Though purely data-driven models are controversial due to lack of physical foundation, neural networks for airfoil flow field prediction are mature (Cao 2024). Thus, it is feasible to predict continuous, high-precision airfoil flow fields within a specific angle of attack range using 2D CFD data of discrete angles of attack as training data. This work proposes a Convolutional Neural Network (CNN) surrogate model, with strong irregular data (e.g., airfoil geometric coordinates and flow field node data) feature extraction ability, which can quickly predict high-precision wind turbine airfoil surrounding flow fields at known angles of attack, with a speed hundreds of times faster than traditional 2D CFD simulations.

On this basis, the lift and drag coefficients of the airfoil at the corresponding angle of attack can be accurately obtained through integral calculation methods based on the predicted flow field results, and these aerodynamic parameters can be directly used to construct the lift and drag database required for the Actuator Line Method, thereby providing efficient and high-precision aerodynamic support for the simulation of wind turbine wakes. To present the research clearly and logically, this paper is organized into several parts. First, the research methodology is described. Next, the neural network structure design, training, and prediction processes are presented. Finally, a summary is provided along with an outlook for future work.

METHODOLOGIES

In this section, the technologies related to CFD simulations used in this study will be introduced, and the verification process will be elaborated.

CFD approach

The numerical simulations in this study are performed using OpenFOAM v2312. The governing equations in this paper are the incompressible Navier-Stokes equations. In the process of constructing a new lift-drag database for the S826 airfoil and calculating the wake of the NTNU BT1, the incompressible Reynolds-Averaged Navier-Stokes (RANS) equations are adopted (Abdollahzadeh 2017):

$$\nabla\cdot \vec{U} = 0 \tag{1}$$

$$\frac{\partial \vec{U}}{\partial t} + \nabla\cdot\left(\vec{U}\,\vec{U}\right) = \nabla\cdot\left[(\nu+\nu_t)\left(\nabla\vec{U} + (\nabla\vec{U})^T\right)\right] - \nabla\left(\frac{p}{\rho} + \frac{2}{3}k\right) + \vec{B} \tag{2}$$

where $\vec{U}$ represents the velocity field, t the time, ρ the air density, p the pressure, $\vec{B}$ the body force vector and k the turbulence kinetic energy. ν denotes the kinematic viscosity of air, and ν_t is the eddy viscosity in the Boussinesq hypothesis which is obtain by solving another two transport equations in two-equation turbulence models, i.e. the turbulence kinetic energy k and specific dissipation rate ω in the k - ω SST model (Menter 2003). The two additional transport equations are as follows:

$$\frac{\partial k}{\partial t} + \nabla\cdot\left(\vec{U}\,k\right) = \tilde{P}_k + \nabla\cdot\left(\Gamma_k \nabla k\right) - D_k \tag{3}$$

$$\frac{\partial \omega}{\partial t} + \nabla\cdot\left(\vec{U}\,\omega\right) = P_\omega + \nabla\cdot\left(\Gamma_\omega \nabla \omega\right) - D_\omega + Y_\omega \tag{4}$$

where $\tilde{P}_k$ and P_ω denote the turbulence production terms, Γ_k and Γ_ω the effective diffusivity of k and ω, respectively. D_k and D_ω are the dissipation terms while Y_ω is the term which blends the standard k - ω and k - ε turbulence models.

CFD simulations

First, in order to construct a high-quality and comprehensive database for the training and validation of the proposed neural network model, this paper systematically carries out detailed computational fluid dynamics (CFD) simulations for the NREL S826 airfoil, a typical wind turbine airfoil widely used in engineering practice. The specific geometric configuration of this airfoil, including its thickness distribution, camber curve, as well as leading edge and trailing edge shapes, is clearly shown in Figure 1 below, providing an intuitive reference for subsequent simulation calculations and experimental comparisons. The NREL S826 airfoil has a standard chord length of 0.45 meters and a span length of 1.78 meters, and its geometric parameters are completely consistent with the design specifications released by the National Renewable Energy Laboratory (NREL), ensuring the authenticity and universality of this research. The Norwegian University of Science and Technology (NTNU) has specially conducted and published model experiment research on this NREL S826 airfoil. To verify the reliability of the CFD simulation results, the simulation results are compared and validated with the published results from NTNU. The experimental setup of NTNU is shown in Figure 2.

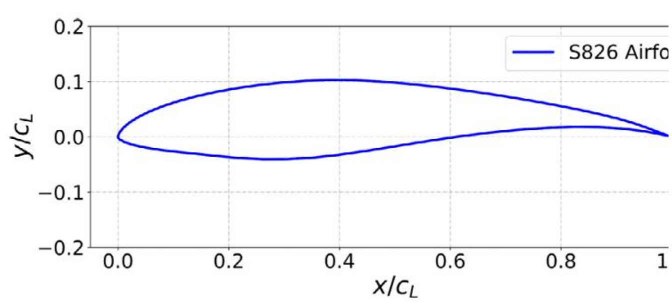

Figure 1 Parameters of the NREL S826 airfoil

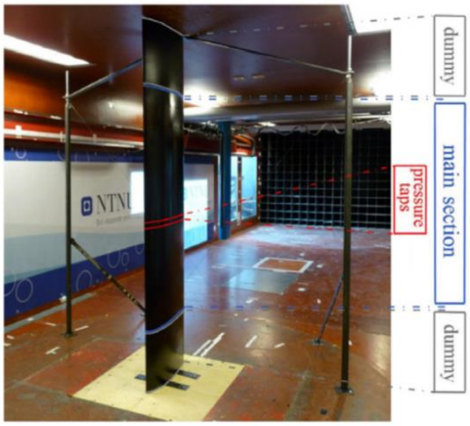

Figure 2 Schematic of the model experiment at NTNU [Bartl 2019]

The airfoil geometry maintains a high degree of uniformity along the spanwise direction, meaning that the cross-sectional shape, thickness distribution, and camber of the airfoil do not change with the spanwise position, which lays a foundation for simplifying the numerical simulation from three-dimensional to two-dimensional. In the experimental process, the two end walls of the test section will inevitably produce boundary layer effects and flow separation phenomena, which will interfere with the flow field around the airfoil and lead to deviations between the measured results and the actual flow characteristics of the airfoil itself. To effectively avoid the adverse influence of the two end walls on the experimental accuracy, the experimental data processing focuses exclusively on the results obtained from the mid-span section of the blade, where the flow field is least affected by the end walls and can most truly reflect the aerodynamic performance of the airfoil. Therefore, corresponding two-dimensional numerical simulations are carried out using the OpenFOAM open-source computational fluid dynamics (CFD) software, with the PimpleFoam solver selected as the core solution tool.

The computational domain for the two-dimensional simulation is carefully designed to ensure that the flow field is fully developed without being restricted by the domain boundaries: the length of the computational domain is set to 12 meters, which is sufficient to accommodate the full development of the inflow and outflow flow fields, while the width is set to 8 meters to avoid the mutual interference between the upper and lower boundaries of the domain and the airfoil flow field. Based on this, three sets of grids with different densities were designed in this study to simulate the condition at an angle of attack of 4° .The maximum Courant number was kept similar and less than 1 for all three grids, based on which the grid convergence analysis was carried out. The results are shown in Figure 4. The airfoil surface pressure coefficient is chosen as the key quantitative comparison index in this validation work; this parameter can directly and intuitively characterize the spatial distribution characteristics of the pressure field on the airfoil surface and is also a core fundamental index for evaluating the overall aerodynamic performance of the airfoil. The quantitative calculation of this coefficient can be realized by the following Equation (5).

$$C_{pn} = \frac{P}{\frac{1}{2}\rho U^2} \tag{5}$$

where p is the pressure, ρ is the air density, and U is the freestream velocity.

It can be seen from the results that when the grid is relatively coarse, the calculated surface pressure near the airfoil leading edge does not converge. Therefore, the medium-density grid is finally adopted. The computational mesh adopts an unstructured cell structure, with a total number of approximately 100,000 cells, which can adapt well to the irregular shape of the airfoil and ensure the rationality of the mesh distribution. To accurately capture the flow characteristics near the airfoil surface, especially the viscous boundary layer and its evolution process, the mesh near the airfoil surface is locally refined with a high density. This local refinement measure is crucial to ensuring that the dimensionless wall distance y+ is less than 1, which is a key prerequisite for accurately simulating the viscous flow near the wall and obtaining reliable aerodynamic parameters such as wall shear stress, as clearly shown in Figure 3 below.

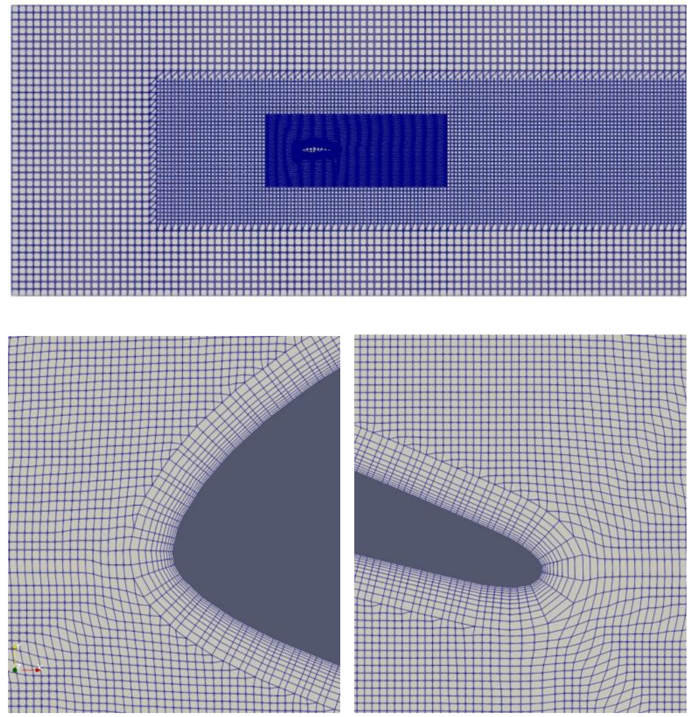

Figure 3 Schematic diagram of meshing

In terms of boundary conditions setting, a no-slip boundary condition is strictly applied on the airfoil surface, which conforms to the actual physical characteristics of the flow field (i.e., the fluid velocity at the solid wall is consistent with the wall velocity, which is zero in this simulation). For other boundaries of the computational domain, zero-gradient conditions are adopted to ensure the smooth development of the flow field and avoid artificial flow field distortion. At the inlet of the computational domain, a fixed velocity boundary condition is specified to simulate the stable inflow state, while a fixed pressure boundary condition is set at the outlet to simulate the atmospheric pressure environment at the downstream of the airfoil, ensuring the rationality of the flow field pressure distribution.

The operating conditions for both the experiment and the numerical simulation are strictly unified to ensure the comparability of the results: the inflow velocity U is set to 3.17 m/s, the turbulence intensity of the inflow is controlled at 0.7% to simulate the low-turbulence environment in the experimental wind tunnel, and the corresponding Reynolds number Re is approximately 100,000, which is calculated based on the chord length of the airfoil and the inflow velocity, belonging to the typical low-Reynolds-number flow range for airfoil aerodynamic simulation.

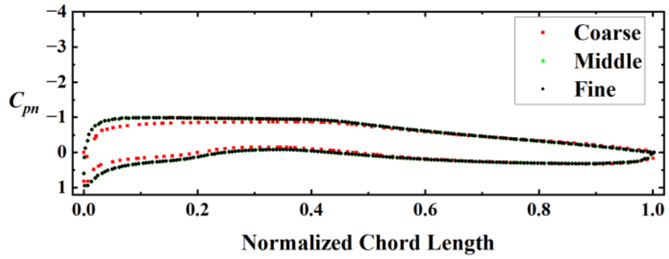

Figure 4 Grid Convergence Analysis

Numerical validation

A rigorous model validation process is conducted in this study to verify the accuracy, reliability and generalization ability of the established numerical simulation model for airfoil flow field prediction. The validation is completed through a comparative analysis with the high-precision experimental measurement data publicly published by the Norwegian University of Science and Technology (NTNU). To comprehensively evaluate the predictive performance of the model under different flow states of the airfoil and cover the typical operating conditions from mild to moderate flow characteristics, the simulation results corresponding to three distinct angles of attack α are specially selected as the core objects for validation analysis, namely the small angle of attack $\alpha = 4^{\circ}$, the moderate angle of attack $\alpha = 8^{\circ}$ and the relatively large angle of attack $\alpha = 8^{\circ}$.

This work systematically compares the numerical simulation results obtained with the pimpleFoam solver against the experimental data published by NTNU (Bartl 2019), verifying the computational accuracy of this numerical method across different angles of attack. The comparison covers three typical angles of attack: $\alpha = 4^{\circ}$, 8°, and 12°.

At $\alpha = 4^{\circ}$, the surface pressure coefficient distribution curve from the numerical simulation shows excellent agreement with the experimental data. Over the entire chord wise range, the two curves exhibit nearly identical trends, with only minor deviations observed in localized regions. As the angle of attack increases to 8°, the pressure gradient on the upper surface of the wing gradually intensifies. Even so, the results from pimpleFoam remain capable of accurately capturing the overall shape of the pressure distribution, with deviations between the numerical and experimental values kept within a small range, both in the pressure peak region and the downstream pressure recovery zone. When the angle of attack is further increased to 12°, flow separation effects begin to emerge, posing higher demands on the precision of the numerical simulation. As can be seen from the figures, the computational results in this study still satisfactorily reproduce the pressure distribution trends observed in the experiments, particularly demonstrating good consistency between numerical and experimental values during the pressure drop phase on the upper surface and the pressure recovery phase at the trailing edge. Overall, the deviations between the numerical simulation results and the experimental data remain within acceptable engineering error limits across all angles of attack. This outcome fully demonstrates that the pimpleFoam solver can accurately simulate the wing surface pressure distribution under different angles of attack. The numerical method exhibits favorable computational accuracy and reliability, providing a solid data foundation for subsequent aerodynamic performance analysis and engineering design.

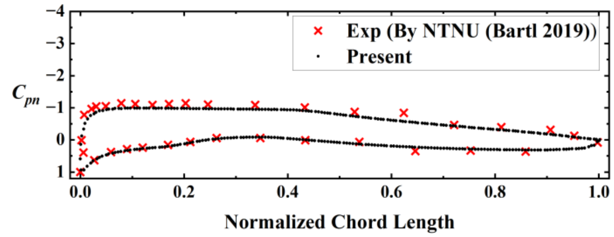

α =4°

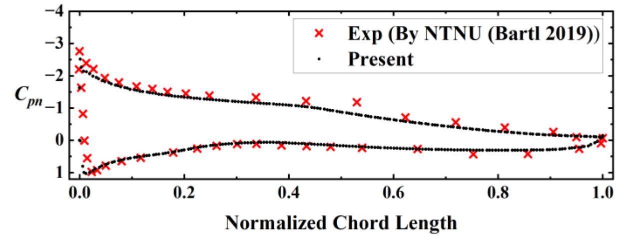

α =8°

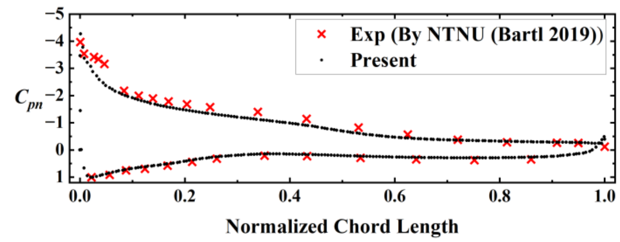

α =12°

Figure 5 Comparison of surface pressure distributions at three angles of attack

The CFD flow field results for these three operating conditions are shown in Figure 6 below. Figure 6(a) shows that the streamlines around the airfoil smoothly adhere to the airfoil surface, with a relatively small velocity difference between the upper and lower surfaces. Figure 6(b) indicates a distinct low-pressure region on the upper surface of the airfoil, along with a pronounced high-pressure area near the leading edge, though the affected area remains relatively limited. Overall, no flow separation is observed, indicating stable aerodynamic performance.

Figures 6(c) and (d) reveal that as the angle of attack increases, the flow velocity on the upper surface of the airfoil rises significantly. The pressure on the upper surface further decreases, and its influence extends over a larger region, suggesting a notable increase in lift. Although no significant flow separation is yet observed, a clear trend of the low-velocity zone near the trailing edge gradually spreading forward can be identified.

As shown in Figures 6(e) and (f), a further increase in the angle of attack causes the flow velocity on the upper surface to reach its peak, while the low-pressure region expands significantly. Theoretically, this indicates that lift reaches a relatively high level. However, the flow field at this stage begins to show signs of instability, with increased disturbances in the wake region, suggesting that flow separation may be imminent or has already initiated to a slight extent. This is typically a characteristic of the airfoil approaching a stall condition.

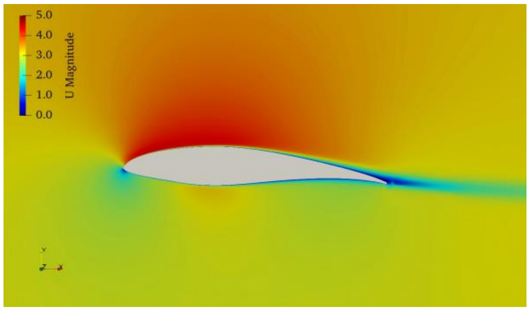

(a) Velocity magnitude contour at α = 4°

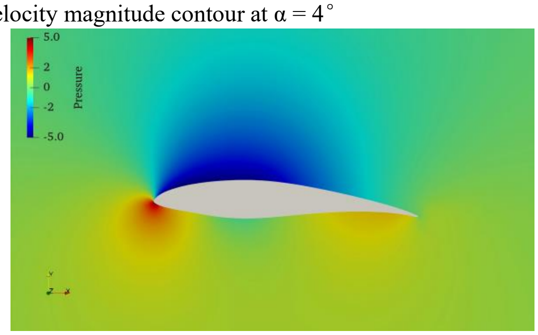

(b) Pressure contours at α = 4°

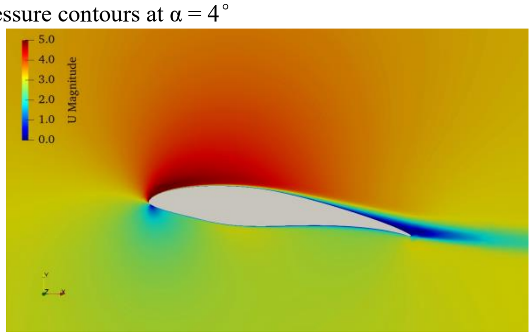

(c) Velocity magnitude contour at α = 8°

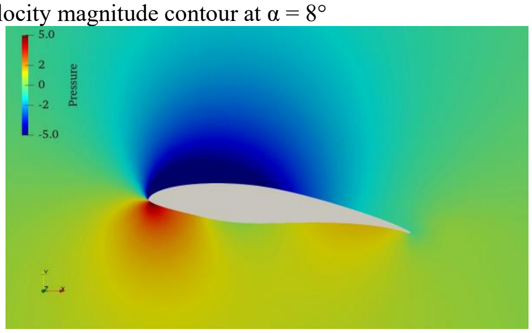

(d) Pressure contours at α = 8°

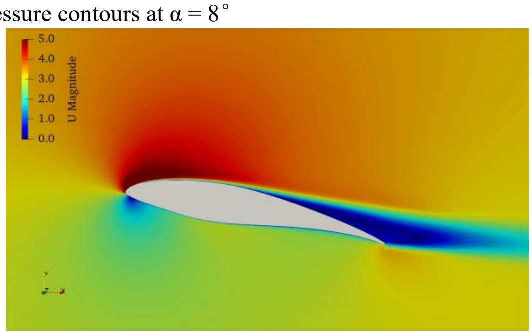

(e) Velocity magnitude contour at α = 12°

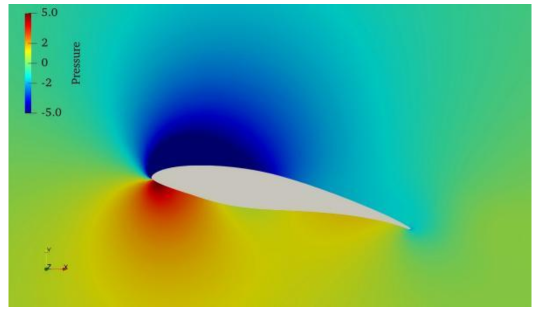

(f) Pressure contours at α = 12°

Figure 6 Velocity magnitude and pressure contours around the S826 airfoil section at Re = 1.0×10^5

NEURAL NETWORK

Dataset calculation

Based on the previously validated mesh and case settings, simulations for other angles of attack were conducted to provide training data for the neural network. Fourteen cases with angles of attack from α = 1° to 14° at an interval of 1° were simulated. The results for α = 4° were designated as the prediction set, while the results for thirteen cases covering α = 1° to 3° and α = 5° to 14° were used as the training set.

For the CNN model used to predict the flow field around an airfoil, the inputs are the airfoil's geometric coordinates and angle of attack α, and the outputs are the flow velocity at each coordinate point and the velocity contour. The flow field prediction results are obtained by the data through the CNN-Attention module. The neural network architecture is shown in Figure 7, and the Tanh function is adopted as the activation function to introduce nonlinearity.

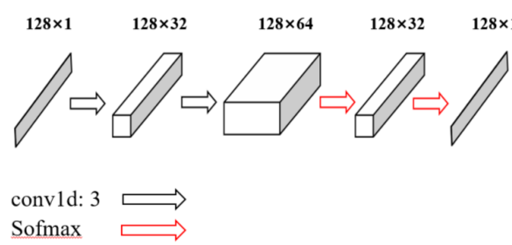

Figure 7 CNN-Attention Architecture

The training process was conducted on a GTX 4060 GPU, with the Adamax optimizer adopted, the learning rate set to 0.0001, and cyclic training performed for 2000 epochs. The MSELoss loss function was used for training, which is defined by the following equation:

$$MSE = \frac{1}{n}\sum_{i=1}^{n}(y_i - \hat{y}_i)^2 \quad (6)$$

The loss function values on the training set and validation set are illustrated in Figure 8.

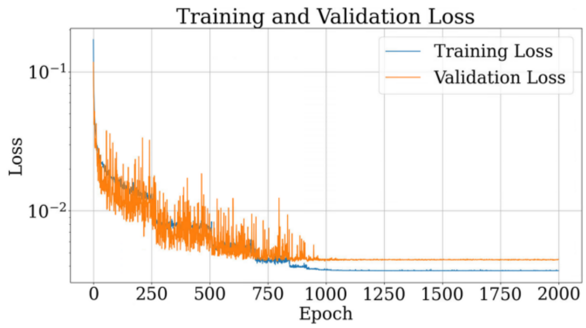

Figure 8 Loss curves of training and validation sets for CNN-Attention

Figure 9 presents the detailed flow field prediction results generated by the CNN-Attention surrogate model for the S826 airfoil at a specific angle of attack of 4°, in direct quantitative comparison with the high-fidelity flow field calculation results obtained from traditional CFD numerical simulations, and also provides a clear visual error distribution contour plot that reflects the magnitude and spatial distribution of the prediction errors between the two sets of results. The comprehensive comparison results fully demonstrate that the proposed CNN-Attention model achieves remarkably high prediction accuracy in capturing the complex flow field characteristics around the airfoil, and its prediction performance is sufficiently reliable to well meet the practical engineering requirements for accurate and efficient airfoil flow field prediction in wind turbine related research.

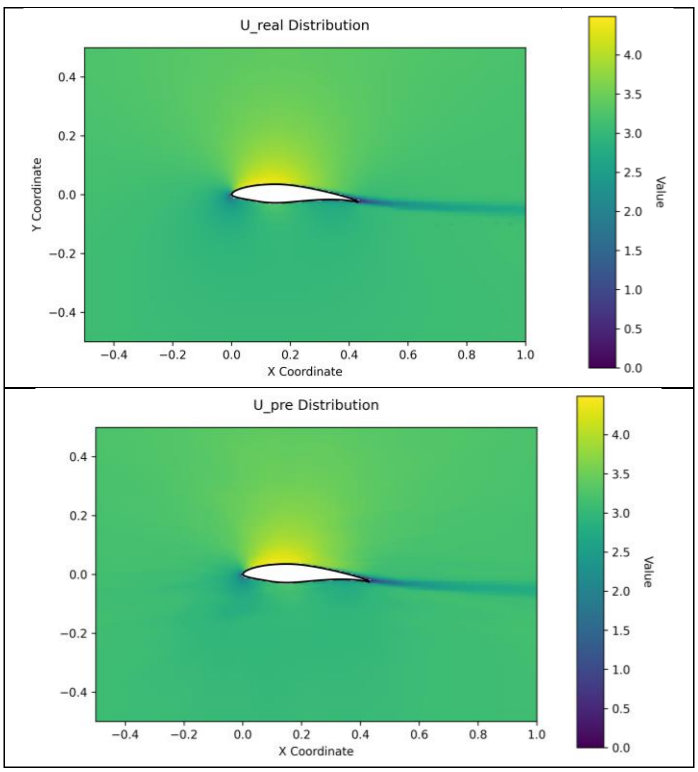

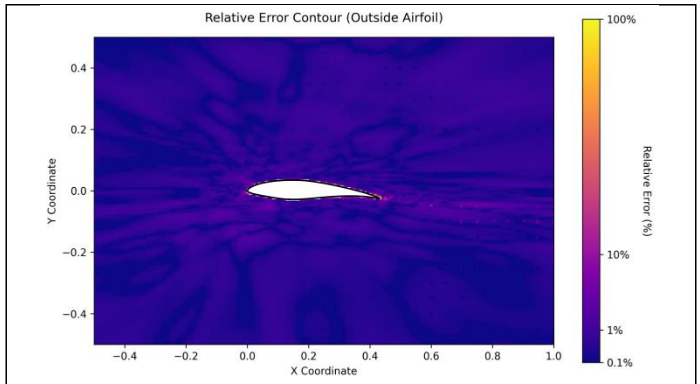

Figure 9 Comparison of prediction results for CNN-Attention

CONCLUSIONS

In this paper, the distribution and numerical results of the surface pressure of the S826 airfoil under different angles of attack α are obtained by using the traditional CFD calculation method. After sorting and screening the results, based on the CNN-Attention model, machine learning training and validation are carried out with the coordinates X, Y and the angle of attack α as input variables, and the flow field results around the airfoil as output variables. The input dataset includes all results except those at $\alpha = 4°$, which is divided into two parts: training set and validation set. After proper parameter tuning and training, the model is used to predict the results at $\alpha = 4°$. The final prediction results are basically consistent with the CFD calculation results and experimental results, which greatly saves calculation time and resources, and also provides an approach for real-time prediction. In the future, on this basis, we will continue to carry out research on the prediction of relevant flow field velocity distribution, and embed the finally trained model into the actuator line model, thereby solving the problem of insufficient accuracy of the actuator line theory to a certain extent.

ACKNOWLEDGEMENTS

This work was supported by the National Key Research and Development Program of China (2025YFF0519800), to which the authors are most grateful.

REFERENCES

Abdollahzadeh, M, Esmaeilpour, R, Vizinho, A, Younesi, and Pàscoa, J, (2017), “Assessment of RANS turbulence models for numerical study of laminar-turbulent transition in convection heat transfer”, International Journal of Heat and Mass Transfer, 115, 1288-1308

Bartl, J, Sagmo, K, Bracchi, T, Sætran, L, (2019), “Performance of the NREL S826 airfoil at low to moderate Reynolds numbers A reference experiment for CFD models”, Eur. J. Mech. B Fluids, 75, 180-192.

Cao, W, Song, J, and Zhang, W, (2024), “Solving high-dimensional parametric engineering problems for inviscid flow around airfoils based on physics-informed neural networks”, Journal of Computational Physics, 516, 113285.

David, A, Saeede, H, Enrico, G, Cristina, H, (2024), “Predicting wind farm wake losses with deep convolutional hierarchical encoder–decoder neural networks”, APL Mach. Learn, 1 March, 2 (1): 016111.

He, R, Yang, H, Sun, S, et al, (2022), “A Machine Learning-Based Fatigue Loads and Power Prediction Method for Wind Turbines under Yaw Control", Applied Energy, 2022, 326.

Jonkman, J, (2003), "Modeling of the UAE Wind Turbine for Refinement of FAST_AD (NREL/TP-500-34755)", National Renewable Energy Laboratory (NREL).

Menter, F, Kuntz, M, Langtry, R, (2003), "Ten years of industrial experience with the SST turbulence model", Turbul. Heat Mass Transf. 4 (1), 625–632.

Peters, N, (2024), "On the Application of an Actuator Line Model for Rotorcraft Outwash Predictions", NASA Technical Report.Muscari, C, Giordani, R and Schito, P, (2023), "On Wind Turbine structural stiffness influence on wake flow", Journal of Fluids and Structures, 118, 103862.

Selig, M, and McGranahan, B, (2001), "Wind Tunnel Aerodynamic Tests of Six Airfoils for Use on Small Wind Turbines (NREL/SR-500-29497)", National Renewable Energy Laboratory (NREL).

Sørensen, J, and Shen, W, (2002). "Numerical modeling of wind turbine wakes", Journal of Fluids Engineering, 124(1), 393–399.

Wang, L, Xie, J, Luo, W, et al, (2022), "Effectiveness of Data-Driven Wind Turbine Wake Models Developed by Machine/Deep Learning with Spatial-Segmentation Technique", Sustainable Energy Technologies and Assessments, 2022, 53.

Ye, M, Hamn-Ching, C, and Arjen, K, (2023a). "High-Fidelity Cfd Simulations for the Wake Characteristics of the Ntnu Bt1 Wind Turbine", Energy, 265.

Ye, M, Chen, H-C, and Koop, A, (2023b), "Verification and validation of CFD simulations of the NTNU BT1 wind turbine", Journal of Wind Engineering and Industrial Aerodynamics, 234, 105336.